Atmos. Chem. Phys. Discuss., 15, 10341–10388, 2015
www.atmos-chem-phys-discuss.net/15/10341/2015/
doi:10.5194/acpd-15-10341-2015
© Author(s) 2015. CC Attribution 3.0 License.

Atmospheric Chemistry and Physics Discussions

This discussion paper is/has been under review for the journal Atmospheric Chemistry and Physics (ACP). Please refer to the corresponding final paper in ACP if available.

Variability of aerosols forecast over the Mediterranean area during July 2013 (ADRIMED/CHARMEX)

L. Menut, G. Réa, S. Mailler, D. Khvorostyanov, and S. Turquety

Laboratoire de Météorologie Dynamique, UMR CNRS 8539, Ecole Polytechnique, Ecole Normale Supérieure, Université P. M. Curie, Ecole Nationale des Ponts et Chaussées, Palaiseau, France

Received: 21 January 2015 – Accepted: 20 March 2015 – Published: 9 April 2015

Correspondence to: L. Menut (menut@lmd.polytechnique.fr)

Published by Copernicus Publications on behalf of the European Geosciences Union.

Abstract

The atmospheric composition was extensively studied in the Euro-Mediterranean region and during the summer 2013, in the framework of the ADRIMED project. During the campaign experiment, the WRF and CHIMERE models were used in forecast mode in order to help scientists to decide whether Intensive Observation Periods should be triggered or not. Each day, a simulation of four days is performed, corresponding to leads from $(D-1)$ to $(D+2)$. The goal of this study is to know the reason why the model does not always simulate in advance what is finally observed: is it due to systematic biases in the models used or to a too large variability due to the real non-linear nature of the meteorology and chemistry? To answer this question, the methodology is to compare the several modelled forecast leads to observations. It was shown that the differences between observations and model is always higher than between the forecast leads. If chemistry-transport model results are not close to the observations, this is mainly due to the model itself (including the meteorology) and its biases. But the forecast variability also acts a lot, mainly due to the modelled wind. This variable is at the origin of the mineral dust and sea salt emissions, as well as the long-range transport of these long-lived species: the wind bias combined to its variability is at the origin of the major part of the aerosols forecast errors.

1 Introduction

The regional air quality was originally focussed on photochemical pollution such as ozone and nitrogen dioxides (Fenger, 2009). This interest was partly motivated by the european "air directives" of 1996, establishing contraints to reduce air pollution for gaseous species only (Monks et al., 2009). More recently, the need of a better understanding of aerosols was added in this regulation framework. If the particulate matter with a diameter less than 10 µm (called PM_{10}) is controlled since many years, the last ten years showed a strengthening of aerosols monitoring, particularly with the

ACPD
15, 10341–10388, 2015

addition of $PM_{2.5}$ routinely measurements (European Union, 2008). In this context, the Mediterranean is well known as an hot spot for this high aerosols concentrations as well as high spatial and temporal variability (Millan et al., 2005).

Aerosols sources and sinks studies remain difficult since a lot of different components are included in these particulate matters: several chemical species or materials (organic matter, sulfates, nitrates, ammonium, mineral dust, sea salt etc.), with several sizes and shapes, several origins in space, lifetimes, potential direct and indirect effects on radiation, cloud formations, etc. In order to reduce potential damages due to too high aerosols concentrations, it is thus necessary to improve our knowledge on all these aspects (Carslaw et al., 2010).

A way to reduce atmospheric pollution is to accurately forecast atmospheric concentrations in order to be able to act at the right time and place to reduce the anthropogenic part of the emissions. This remains today a challenge and forecast systems often miss large pollution events. Some previous studies tried to identify and thus reduce the forecast error. For example, Manders et al. (2009) quantified the capability of the LOTOS-EUROS system to forecast PM_{10}. By reducing some systematic identified biases, Borrego et al. (2011) showed the forecast could be improved over Portugal. Another way to improve forecast is to reduce biases by increasing realism in the aerosols representation: this was conducted in Mulcahy et al. (2014) for the Met Office global numerical weather prediction model, showing a benefit on the forecast scores. More recently, several studies showed that data assimilation may reduce the forecast error by constraining the forecast initial conditions, as in Niu et al. (2008) and Curier et al. (2012). For all these studies, bias and variability were treated together. Other framweorks provide daily experimental forecast such as DREAM (Pérez et al., 2007) and SKYRON (Spyrou et al., 2013) but they mainly focussed on mineral dust.

In the present study, we propose to estimate the relative contributions of two modelling aspects, the bias and the variability, by comparing several forecast leads to observations. The main question is *to what extent the differences between observed and modelled concentrations are due to the model errors or to the real non-linear variability*

ACPD
15, 10341–10388, 2015

of the atmospheric system to represent? To answer this question, we take advantage of the CHARMEX program (Dulac et al., 2013), and more precisely to the ADRIMED project, studying the atmospheric composition during June and July 2013 and over the Mediterranean area (Mallet, 2015). During the months of June and July 2013, the ADRIMED project experimental part was conducted to document the atmospheric composition in the Western-Mediterranean region. In parallel to these measurements, regional models were used in real-time forecast to help the instrumental teams to define when and where the best measurements can be done. In this case, the models are not used to analyze the meteorology and chemical composition during a long period but only to quickly provide informations about the current state of the atmosphere and its probable evolution during the next days.

The present study was done using the same measurements and models configurations than the ones presented in Menut et al. (2015). The added value in the present study is the use of this modelling plat-form in a forecast mode. Section 2 summarizes the sites from where observations are used. Section 3 presents the modelling system and the forecast set-up. Sections 4 and 5 present the variability of the forecasted meteorological fields and pollutants emissions, respectively. Section 7 presents aerosols concentrations results and their variability as maps and for selected sites using time series and vertical profiles, compared to the available measurements. Conclusions and perspectives are presented in Sect. 8.

2 The observations

In this study, the observations used are the same as those used in Menut et al. (2015): the AERONET hourly measurements (Dubovik and King, 2000), for the Aerosol Optical Depth (AOD) and the EEA network data (Guerreiro et al., 2013), for the surface PM_{10} concentrations. All the measurements sites locations used in this study are summarized in Table 1: for each site, the longitude, latitude and altitude above sea level (a.s.l.)

ACPD
15, 10341–10388, 2015

are presented. In addition, specific measurements performed during the ADRIMED campaign and located at Lampedusa and Cape Corsica are added to the analysis.

3 The modeling system

The modeling system is composed of several models: the WRF regional meteorological model, the CHIMERE chemistry-transport model and additional individual models for emissions fluxes estimations. All these models are integrated in a modelling plat-form usable both in analysis and forecast mode. We first describe the whole modelling plat-form, including the forecast configuration, then the models WRF and CHIMERE. This modelling plat-form is strictly the same than the one extensively described in Menut et al. (2015).

3.1 The forecast configuration

Even if the WRF and CHIMERE models have regurlarly new versions, the forecast configuration of these models remains the same and was previously used in many studies as listed in (Menut and Bessagnet, 2010). More precisely, this forecast configuration was used during the ESCOMPTE project in the south of France (Menut et al., 2005) and during the AMMA experimental campaign for mineral dust aerosols in western Africa (Menut et al., 2009). CHIMERE is also used in an operational context since 2003 for the PREVAIR French air quality forecast (Honoré et al., 2008; Rouïl et al., 2009), and in the MACC European project (Inness et al., 2013).

This forecast system is presented in Fig. 1. The first step is to calculate forecasted regional meteorology. The global GFS/NCEP forecast fields are used to force the regional WRF3.5.1 model (see detailed description below) and from $(D-1)$ (i.e. the day before) to $(D+2)$ (two days in advance). They are then used for several calculations: (i) the surface emissions fluxes, (ii) the transport and mixing of gaseous and aerosols species with CHIMERE. For the specific case of the vegetation fires emissions, satellite

ACPD
15, 10341–10388, 2015

observations of fire activity (MODIS near-real time detection) during the previous day are analyzed to derive the corresponding area burned. These are then used as input to the high resolution fire emissions model (Turquety et al., 2014), assuming fires will continue burning during the first 72 h of the forecast period. The biogenic and mineral dust emissions fluxes depend on the meteorology, when the anthropogenic emissions are only dependent on the week day. The initial conditions for gas and aerosols concentrations are taken from the forecast of the day before. In practice, this means that the system was launched several days before the first day for the first forecast of the period and in order to have a correct spin-up.

In this study, the simulation was performed from 10 June to 5 July 2013. Each day, a simulation of four days is performed, from ($D-1$) to ($D+2$). For each modelled period, meteorological parameters, gas and aerosols species are hourly calculated on the domain grid. Thus, for each of these parameters, each grid cell and each hour of the period, this allows to have four different values. By comparing these four values, we can quantify the forecast variability. For the results analysis, the focus will be done on the period ranging from the 14 to the 26 June 2013, identified as the period with the most interesting pollution events during the ADRIMED project.

3.2 The meteorological model WRF

The meteorological parameters are modelled with the WRF regional model in its version 3.5.1. The model is used in its non-hydrostatic configuration, with a constant horizontal resolution of 60 km × 60 km and 28 vertical levels from surface to 50 hPa. The Single Moment-5 class microphysics scheme is used allowing for mixed phase processes and super cooled water (Hong et al., 2004). The radiation scheme is RRTMG scheme with the MCICA method of random cloud overlap (Mlawer et al., 1997). The surface layer scheme is based on Monin-Obukhov with Carslon-Boland viscous sublayer. The surface physics is calculated using the Noah Land Surface Model scheme with four soil temperature and moisture layers (Chen and Dudhia, 2001). The planetary boundary layer physics is processed using the Yonsei University scheme (Hong

ACPD
15, 10341–10388, 2015

et al., 2006) and the cumulus parameterization uses the ensemble scheme of Grell and Devenyi (2002).

The global fields of NCEP/GFS are hourly read by WRF using nudging techniques and for the main atmospheric variables (pressure, temperature, humidity, wind). In order to preserve both large-scale circulations and small scale gradients and variability, the "spectral nudging" was chosen. This nudging was evaluated in regional models, as presented in Von Storch et al. (2000). In this study, the spectral nudging was selected to be applied for all wavelength greater than ≈ 2000 km (wavenumbers less than 3 in latitude and longitude, for wind, temperature and humidity and only above 850 hPa). This configuration allows the regional model to create its own structures within the boundary layer but to follow the large scale meteorological fields.

3.3 The chemistry-transport model CHIMERE

CHIMERE is a chemistry-transport model able to simulate concentrations fields of gaseous and aerosols species at a regional scale. The model is off-line and thus needs pre-calculated meteorological fields to run. In this study, we used the version fully described in Menut et al. (2013a). The horizontal domain is the same as the one of WRF. For the vertical grid, the 28 vertical levels are projected onto the 20 levels of the CHIMERE mesh.

The gaseous species are calculated using the MELCHIOR 2 scheme and the aerosols using the scheme developed by Bessagnet et al. (2004). This module takes into account species such as sulphate, nitrate, ammonium, primary organic (OC) and black carbon (BC), secondary organic aerosols (SOA), sea salt, dust and water. These aerosols are represented using nine bins, from 40 nm to 20 µm, in diameter. The life cycle of these aerosols is completely represented with nucleation of sulphuric acid, coagulation, adsorption/desorption, wet and dry deposition and scavenging. This scavenging is both represented by coagulation with cloud droplets and precipitation. The formation of SOA is also taken into account.

ACPD
15, 10341–10388, 2015

The anthropogenic emissions are estimated using the same methodology as the one described in Menut et al. (2012) but with the HTAP masses as input data. These masses were prepared by the EDGAR Team, using inventories based on MICS-Asia, EPA-US/Canada and TNO databases (http://edgar.jrc.ec.europa.eu/htap_v2/index.php?SECURE=123). Biogenic emissions are calculated using the MEGAN emissions scheme (Guenther et al., 2006) which provides fluxes of isoprene, terpene and pinenes. In addition to this version, several processes were improved and added in the framework of this study. First, the mineral dust emissions are now calculated using new soil and surface databases, as described in Menut et al. (2013b). Second, chemical species emissions fluxes produced by vegetation fires are estimated using the new high resolution fire model presented in Turquety et al. (2014). And, finally, the photolysis rates are explicitely calculated using the FastJ radiation module, (Wild et al., 2000) and as fully described in Mailler et al. (2015).

4 Predictability of meteorological parameters

Due to many processes, the atmospheric concentrations of trace gases and aerosols are very sensitive to the meteorological fields. First, some of the sources are directly dependent on the near-surface meteorology: (i) the mineral dust emissions depend on the surface wind speed, (ii) the biogenic emissions depend on temperature and radiation, and (iii) the fires emissions depend on the soil moisture (for fire efficiency) and the boundary layer dynamics (for the pyroconvection). Second, during the transport, the atmospheric species will be under the influence of: (i) the wind, pressure, humidity and temperature for the boundary layer dynamics and tropospheric long-range transport and (ii) the clouds and radiation attenuation for the photochemistry. Finally, the sinks of atmospheric species are mainly (i) the surface layer turbulence acting on gas and aerosols dry deposition and, (ii) the precipitations by the way of aerosols scavenging. In order to understand the several types of meteorological variabilities influencing ozone and aerosols concentrations, we focus on temperature, wind speed and precipitations.

ACPD
15, 10341–10388, 2015

4.1 Variability of 2 m temperature

The variability of the 2 m temperature is studied using statistical scores and direct interpretation of time series for selected sites. The modelled 2 m temperatures are extracted for two kind of locations. First, European stations where E-OBS data are available (listed in Table 2). In this case, comparisons to the measurements are presented. Second, the three sites of Banizoumbou, Cape Corsica and Lampedusa, being of interest for other dependent variables as the mineral dust, sea salt and biogenic emissions. In this case, comparisons are done between the modelled results only in order to quantify the variability of the model between the several forecast leads.

4.1.1 Statistical scores for 2 m temperature

Table 2 present scores for the comparison between the E-OBS data and the corresponding model values. The several forecast leads are compared to the observations using correlation R and absolute bias. In general, the correlations between measurements and modelled values are always good with values higher than 0.74. The bias is mainly negative with values between 0.7 (Bastia) to −4.02 K (Champforgeuil) for the $(D-1)$ simulation. This shows, in general, that the model underestimates the mean daily 2 m temperature over the whole simulation domain.

The correlation values decrease when the forecast lead increases: this is a logical result, the uncertainty growing with the forecast lead. For example, the correlations ranges from 0.81 to 0.79 in Cape Corsica, 0.96 to 0.90 in Baceno, 0.89 to 0.79 in Vercelli. On the other hand, surprinsingly, the bias decreases with the forecast for all studied stations (except Bastia). It is difficult to find a clear reason for this behaviour and there is no information available which may help explaining this result.

ACPD
15, 10341–10388, 2015

4.1.2 Time series of 2 m temperature

Time series of observed and modelled daily mean averaged 2 m temperature are displayed in Fig. 2. These time series are presented as examples of the results discussed before and are for the Zorita (Spain), Agen (France) and Vercelli (Italy) sites. The systematic model underestimation clearly appears. But, over the whole period, the model shows its ability to model the weekly variability i.e. is able to reproduce the main synoptic circulations: this is certainly the most important point for the modelling of emissions and long-range transport of pollutants over this large region including North of Africa and Europe.

Figure 2 shows that the variability between the forecast leads is lower than the differences between the observations and the model. In order to better see the differences between the forecast 2 m temperature time-series, Fig. 3 presents the percentages of differences between the forecast ($D+0$), ($D+1$), ($D+2$) and the "analysis" fields, ($D-1$). These figures, (unlike the daily mean of Fig. 2), are here with hourly values of the 2 m temperature in order to see the hourly variability.

Three sites are chosen for this comparison and they were selected as sites representative of very different locations in the domain: Banizoumbou, Cape Corsica and Lampedusa. These are also sites where E-OBS data are not available, being in Africa and over islands in the Meditteranean. Note that these percentages are calculated using temperature values in Kelvin. The maximum differences are calculated for Banizoumbou: over the whole period, values range from ≈ -2 to $+2$ % (i.e. for a mean value of 300 K, a variability of ± 6 K). In Cape Corsica, the maximum differences are lower and ≈ -0.5 to $+0.5$ %. Finally, in Lampedusa, the differences may be considered as negligible with values less than 0.2 % (i.e. less than 0.6 K).

4.2 Variability of the wind speed and direction

The wind speed is a key factor in meteorology and chemistry-transport modelling. Close to the surface (represented by the 10 m wind speed), this variable will drive

ACPD
15, 10341–10388, 2015

the mineral dust and sea salt emissions as well as the diurnal cycle of the convection in the boundary layer. In altitude, horizontal transport is constrained by this variable. In order to quantify the wind variability, several forecast leads are first compared in terms of 10 m wind speed times series. Second, vertical profiles are compared. Note that for these two comparisons, there are no measurements available.

4.2.1 Time series of 10 m wind speed

The 10 m wind speed, $|U|_{10\,m}$, is an important parameter for numerous processes affecting the atmospheric composition: its value is directly used in many model parameterizations as the saltation and sandblasting processes, driving the mineral dust emission fluxes. This is also a key parameter for the estimation of dry deposition velocities. Close to the surface, the wind speed varies a lot naturally, depending on the atmospheric stability as well as the horizontal heteorogeneity of the studied location.

The variability of $|U|_{10\,m}$ is quantified, for comparison, at the same sites as those used for the 2 m temperature. Results are displayed in Fig. 4 for these sites with the modelled absolute values on the left panel and the variability on the right panel. This variability is expressed as a percentage of differences between the $(D-1)$ forecast and the other forecasts ($D+0$, $D+1$ and $D+2$). In order to avoid unrealistic values due to wind speed close to zero, the calculations of the percentages are done only for values $|U|_{(D-1)} > 0.1\,m\,s^{-1}$.

Compared to the 2 m temperature, the 10 m wind speed variability is very high. There is no specific systematic bias and the values of differences ranged from 0 to 250 %, for wind speed between 0.1 and $10\,m\,s^{-1}$. For the site of Banizoumbou, mineral dust emissions will be sensitive to this wind speed and its variability. It is known that saltation occurs for wind speed values up to $\approx 6\,m\,s^{-1}$ (even if this absolute value may depend on the soil texture and the landuse). A variability of $\pm 1\,m\,s^{-1}$ (low in absolute value), as observed in the Banizoumbou time series, may have a large impact on mineral dust emissions fluxes. For the sites of Cape Corsica and Lampedusa, the mineral dust emissions are lower than in Africa. In this case, the dry deposition may become

ACPD
15, 10341–10388, 2015

one of the most sensitive parameters. Values of variability are more moderate than in Banizoumbou but still very high: with values up to 150 % in Cape Corsica and 130 % in Lampedusa.

4.2.2 Vertical profiles of wind speed and direction

Figure 5 presents vertical profiles of mean wind speed and wind direction for two locations corresponding to the Cape Corsica and Lampedusa ADRIMED super-sites. The profiles are presented for the whole atmospheric column modelled by CHIMERE, from the surface to 8000 m a.g.l. and for the 18 and 21 June 2013 at 12:00 UTC.

For the 18 June, the wind speed is lower than for the 21 June over the two sites. For the two sites and the two days, the values are close between ($D-1$) and ($D+0$). On the contrary, large differences appear between ($D-1$) and the forecasts at ($D+1$) and ($D+2$). For example, on 18 June at Cape Corsica, in the lower troposphere, the wind speed is lower than 6 m s^{-1} for ($D+1$) and ($D+2$), while the values are around 8 m s^{-1} for ($D-1$) and ($D+0$). In this case, the forecasted transport is lower and may induce air masses being not transported at the right time in this area. On the contrary, while the modelled wind speed seems to have a low variability and low values for ($D-1$), ($D+0$) and ($D+1$) in Lampedusa and for 21 June, the ($D+2$) forecast shows larger values: for an altitude around 3000 m a.g.l., the wind speed varies from 2 to 10 m s^{-1}. In this latter case, the forecasted aerosol plumes could be advected too fast in the middle of the Mediterranean.

The wind direction also exhibits a large variability. For long-range transport of aerosol plumes, the largest variability is modelled in Lampedusa for the 18 and 21 June and for altitudes between 2000 and 4000 m. For the other sites and days, the wind direction variability is smaller in the low troposphere. In altitude, a very strong forecast variability is modelled in Cape Corsica, for the 18 June: but this variability is up to 6000 m, and aerosol concentrations are low in this part of the troposphere.

ACPD
15, 10341–10388, 2015

4.3 Variability of precipitations

Results of Hit Rates and biases between the E-OBS observations and modelled values are presented in Table 3. The Hit Rates are calculated as described in Menut et al. (2015), for the same period, region and data. Note that the number of studied sites is reduced compared to the 2 m temperature: this is just because no precipitation was recorded for some sites, leading to the impossibility to quantify scores. For the sites where precipitation amount was observed and/or modelled, the results showed that this variable is correctly modelled in time frequency, but less in magnitude. The Hit Rates vary from 0.33 (in Gap) to 1 for $(D-1)$ compared to the observations. These scores are the same or worse for the comparison between the E-OBS observations and the $(D+2)$ simulation, with values ranging between 0.25 to 1. Biases are often high: for $(D-1)$, the bias range from -7.80 to $+3.09\,\mathrm{mm\,day^{-1}}$. From $(D-1)$ to $(D+2)$, these bias values logically increase ranging between -8.53 to $+4.95$.

To quantify the Hit Rates and bias results in terms of magnitude and time, three time series are presented, Fig. 6. Zorita (Spain), Agen (France) and Vercelli (Italy) are considered as representative of the behaviour observed over all stations and were also already presented for the discussion about the 2 m temperature.

In Zorita, three precipitation events are observed during the period: two events are modelled and one missed. For the two modelled events, the model mainly overestimate the precipitation amount. The strong bias for this station is mainly due to: (i) the 17 June where a precipitation of $11\,\mathrm{mm\,day^{-1}}$ is observed but not modeleld and (ii) the 19 June, where the model diagnosed a precipitation that has not been observed. In Agen, five precipitations events are observed, correctly modelled in terms of time period, but less in magnitude. In this case, the model underestimates the observations, leading to a systematic negative bias, as reported in Table 3. At the end of the period, the model overestimates the precipitation but with very low values, not able to counterbalance the large underestimation of the beginning of the period. Finally, in Vercelli,

ACPD
15, 10341–10388, 2015

three precipitation events were observed. They are well modelled for the corresponding days with a moderate underestimation by the model.

Globally, when a precipitation event is observed, it is often reproduced by the model. The precipitation intensity appears more difficult to simulate and a factor of 2 (under- or over-estimation) is often found. A large variability is found between the forecast lead in terms of magnitude but not in terms of days with or without precipitation. For a chemistry-transport model, independently of the meteorology, the time occurence is more important than the magnitude: the scavenging schemes leading to a global cleaning of the atmospheric column under a diagnosed precipitating cloud. Thus, with these results, it appears that the most sensitive aspect, the time frequency, is sufficiently well modelled, even if the magnitude is certainly not.

5 Predictability of emissions

In this section, the predictability of emissions is quantified for the mineral dust and biogenic emissions. Anthropogenic emissions are not hourly or daily meteorology-dependent and their variability is thus not considered here. For the fire emissions, the model is not able to forecast the burned areas in advance. Each day, the burned areas of the day before are used for the whole period to forecast: the main varying parameter is kept constant. In addition, no significant fire events occurred in June 2013. The fires emission variability is thus not considered too.

5.1 Variability of mineral dust emissions

Mineral dust emissions depend on the soil texture, the surface with the landuse and the surface layer wind speed. At the regional scale and during a few days, there is no variability of the soil and surfaces characteristics. On the other hand, the surface layer wind speed can vary a lot. Mineral dust emissions are strongly dependent on the wind speed and, thus, the corresponding friction velocity u_* (Menut et al., 2013b).

ACPD
15, 10341–10388, 2015

These dynamical variables act in a non-linear way: the mineral dust emission occurs only if the friction velocity is greater than a threshold value, u_*^T, itself depending on the surface characteristics. This means that for a small change, ϵ, in the friction velocity value (parameterized using the 10 m wind speed), the mineral dust emission could be zero (if $u_* = u_*^T - \epsilon$) or not (if $u_* = u_*^T + \epsilon$).

Figure 7 presents two maps for the mineral dust fluxes. Even if this model version allows the calculation of the mineral dust fluxes over Europe, and with the same scheme as over Africa, the largest fluxes are calculated over Africa. The map for the 20 June 2013 is shown as an example, after daily cumulating the hourly fluxes calculated by the model. For this day, the emissions are mainly over western Africa and Saudi Arabia. Depending on the location, these fluxes range from 0.1 to more than 20 $g\,m^{-2}\,day^{-1}$. The second map shows the differences between the fluxes calculated for the same day but at several forecast leads: $(D-1)$ and $(D+2)$. For the region where the highest fluxes are estimated, the absolute differences may be very large i.e. of the same order of magnitude as the flux itself.

In order to quantify this variability in a synthetic way, the mineral dust emissions fluxes are daily cumulated over the whole simulation domain. The values are presented in Fig. 8 top and are thus expressed in $Tg\,day^{-1}$. These results show that the variability is close between the several leads: the two main peaks are modelled for the 25 and 28 June with the same order of magnitude. These fluxes being mainly wind speed dependent, this means that the model is stable at the synoptic scale and the mean large scales wind variability is reproduced regardless of the forecast lead. Looking in more detail, some differences are present for each day. For example on 22 June, the modelled fluxes are relatively low but highly variable.

The same results are expressed in relative differences in Fig. 8 bottom. The sign of these differences is not constant in time, showing a large variability from day to day. The maximum values of differences are ±30 % of the maximum daily flux. Logically, the greater the forecast lead (i.e. for $(D+1)$ and $(D+2)$), the larger the differences are important.

ACPD
15, 10341–10388, 2015

Finally, even if the forecast is variable, when a high wind speed is forecasted, this is generally true for all leads: in this case, fluxes occur for all forecast leads. This means that the largest differences are not always for highest fluxes, but can also occur when the wind speed is close to the threshold value.

5.2 Variability of biogenic emissions

The biogenic emissions are sensitive to the temperature and the photosynthetic active radiation (PAR). Over vegetative areas, some changes in these meteorological values could impact the isoprene and terpenes emissions fluxes. As for the dust emissions, the biogenic emissions are cumulated over the whole simulation domain. The time series are presented in Fig. 9 top. A moderate day to day variability is modelled over the whole period: starting with a low value of 2.2×10^9 molecules day^{-1}, a maximum of 2.4×10^9 molecules day^{-1} is reached on 17 June, following by a monotonic decrease to 1.8×10^9 molecules day^{-1}.

For all forecast leads, this variability is modelled in the same way. The relative differences, in %, are displayed in Fig. 9 bottom. For all leads and all days, the same tendency is observed: the greater the forecast lead, the larger the fluxes. But, while the maximum of variability is between $(D-1)$ and $(D+2)$, with peaks around +6 %, these differences are lower for the other days: in average +4 % for $(D+1)$ and +2 % for $(D+0)$. The overall variability of biogenic emissions is low, with maximum values of 6 %, consistent with that of the temperature, the latter being its main driver.

6 Predictability of aerosols optical depth

Before an analysis of the aerosol concentrations, a first evaluation is presented here for the Aerosol Optical depth (AOD). The AOD corresponds to the impact of all aerosols, in the whole atmospheric column, on the radiation at the surface. The AOD may be

ACPD
15, 10341–10388, 2015

available using satellite data analysis and inversion of photometers data. In this section, the AERONET level 2 data are used.

6.1 Variability of AOD time series

Time series of AOD for selected sites are presented in Fig. 10. The AERONET observations are compared to the four forecast leads from ($D-1$) to ($D+2$). Hourly values are presented to better explain the large variability of the measurements compared to the modelled values.

In Banizoumbou, the measurements are representative of a site close to the mineral dust sources. Large values of AOD are measured and not modelled. Over the whole period, from 14 to 30 June, two events of large AOD are measured corresponding to the 15 and 21 June. The model is able to reproduce these peaks, but not with the correct timing for the first peak, being modelled on 16 June. For the 21 June peak, only the ($D+1$) forecast shows a significant increase of the modelled AOD value. In Capo Verde, the available measurements are less numerous. The trend in the observations is reproduced by the model with rather low values between 0.1 and 0.8. A large variability is modelled between the forecast leads, as for the period from 22 to 24 June. In Lampedusa, a site in the middle of the Mediterranean sea and under mineral dust plumes, the main variability over the whole period is well reproduced: the main peak is observed on 24 June and the modelled values are also maximum for this day. The variability between the forecast leads is here moderate.

By comparing the observations and the model, it is clear that the forecast variability is always lower than the differences between model and observations. In order to quantify this variability between model and observations, correlation is calculated for each forecast lead and results are presented in Table 4. As well as for time series, calculations are done for hourly values. First, it appears that results are less good than the ones presented in Menut et al. (2015) for the same sites, the same observations and the same model. The differences between the two studies is the studied period length: in Menut et al. (2015), observations and model are compared from 1 June to

ACPD
15, 10341–10388, 2015

15 July 2013, i.e. 45 days. In this study, and since many forecast leads are analyzed, the period reduces to 15 days. This may be explained by the fact that AOD correlations are mainly driven by the transport of dense plumes that have a natural variability of the order of several days. In the case of this study, two weeks of forecast represent one to two possible plumes events: the correlation scores thus become very sensitive to the model ability to catch these events or not.

Results presented in Table 4 show that the correlation is not decreasing with forecast leads as one would expect. For example, in Capo Verde, the best correlation is found for (D+2) with a value of 0.448. This is much larger than the (D−1) lead with 0.343 and (D+1) with 0.134. These differences are mainly due to the fact that the model reproduces two small peaks for (D + 2) (16 and 23 June), not modelled for the other leads. The highest correlations found for (D − 1) are only calculated for Izana and Lampedusa.

6.2 Variability of AOD maps

The AOD time series were used to compare the model results to the observations. In order to have another view of these results, AOD maps are presented in Fig. 11. An evaluation of the model capability compared to satellite data was already presented and discussed in Menut et al. (2015), showing that the model is able to reproduce the main large-scale AOD patterns as well as the absolute values of these AOD. On this figure, the daily averaged AOD is presented for the 20 June as an example. This day was identified as one with an important plume of mineral dust flewing from Africa to the South of Europe. The highest AOD peaks are located in Western Africa and Saudi Aarabia, with maximum values of ≈ 1.8. The plume over Europe shows values between 0.1 and 1. The three other maps represent the absolute difference between the daily averaged map of 20 June (D − 1) and the forecast leads for the same day: (D + 0), (D + 1) and (D + 2). Logically, the greater the forecast leads the greater the differences between them.

First, these maps show that the largest differences are located in Africa where mineral dust are emitted and where the highest AOD are calculated, such as the hot spots

ACPD
15, 10341–10388, 2015

located in Senegal and Yemen. The differences appear as plumes, highlighting the fact that they are due to emissions but also to transport.

Another interesting point is that these differences are not spatially homogeneous. Positive and negative differences are observed and these dipoles increase with the forecast lead. These gradients are located where the most important AOD are modelled. These locations correspond to largest emissions and transport of mineral dust. The mineral dust being very sensitive to the wind (speed and direction), the gradients reflect the impact of the wind direction variability from one forecats lead to the next one.

After long-range transport, the differences may also appear negative or positive: the longer the transport of dense plumes the more the differences will be pronounced. Finally, for AOD values ranging between 0 to 2, the absolute differences between all forecast leads may reach ±0.1, i.e. ≈ 10 %.

7 Predictability of surface PM_{10}

The predictability is presented here for surface concentrations, including comparison to routine surface measurements of the EEA network. The hourly values are used for time series and statistical scores for the selected sites where measurements are available.

7.1 Time series of hourly surface PM_{10}

Time series of hourly surface concentrations of PM_{10} are displayed in Fig. 12 for the sites of Lampedusa, Zorita and Cartagena, as examples. In Lampedusa, several periods with high values of PM_{10} are recorded: 16 June and the period between 24 and 27 June. For the observed peak of 16 June, the PM_{10} concentration is $\approx 60\,\mu g\,m^{-3}$. The model is not able to reproduce this event, staying with low values of $\approx 20\,\mu g\,m^{-3}$. For the second peak, with values up to $\approx 100\,\mu g\,m^{-3}$, the model reproduces a surface concentration peak, but only during a few hours of the 24 June. In Zorita, only one peak is observed during the period and for the 19 June. In this case, the model is able to

ACPD
15, 10341–10388, 2015

reproduce this peak in time, but the modelled values are overestimated: the maximum observed value is $\approx 50\,\mu g\,m^{-3}$ when the model simulates values $\approx 80\,\mu g\,m^{-3}$. However, all leads are not reproducing this peak, since the $(D+1)$ lead shows values less than $20\,\mu g\,m^{-3}$ for this day. The model also shows a second peak during the 18 June, but no measurements are available for this day. Finally, the comparison for the Cartagena site is an example of the unability of the model to correctly reproduce an observed peak: while the highest values are observed during the 20 to 22 June period, the only modelled peak occurs the 18 June.

7.2 Correlation for hourly surface PM_{10}

In order to have a synthetic view of the forecast variability compared to the observations, statistical scores of correlation are presented in Table 5. The scores are calculated using the hourly surface concentration values of PM_{10}. The correlations values are varying a lot from one site to another. But for one specific site, the correlations remains close. In addition, and as for the AOD results, the best correlations are not found for the forecast $(D+0)$, as one might expect. This confirms the fact that the ability of the model to correctly reproduce the surface PM_{10} variability is not determined, to the first order, by the forecast variability.

7.3 Vertical profiles of sea-salt and mineral dust

Vertical profiles of mineral dust and sea salt are presented in Fig. 13, respectively. These figures offer another view of the modelled concentrations variability. These two species have in common to mainly depend on the surface wind speed for their emissions. But, after being emitted they have different lifetimes, depending on the source region, the meteorology and the chemistry. Profiles are displayed for the 18 and 21 June, and for the two sites of Cape Corsica and Lamdepusa: the same locations and dates as for the wind speed and direction as presented in Fig. 5, for a direct comparison.

ACPD
15, 10341–10388, 2015

The mineral dust profiles show, for the two sites and the two days, that the highest concentations are in altitude, between 1000 and 5000 m. This makes sense since these mineral dusts were mainly emitted in Africa, far from these sites. The variability between the forecast leads is huge. For example for 18 June above Cape Corsica, the concentrations are relatively low except for ($D+2$) where a very large peak is forecasted: more than 80 $\mu g\,m^{-3}$, when the other leads have maximum values of 20 $\mu g\,m^{-3}$. One can also note that the ($D-1$) and ($D+0$) leads show the same vertical profile of concentrations. The opposite result is shown in Lampedusa for June, 21: while the $D-1$ and $D+0$ are also similar, the $D+2$ vertical profile is lower in this case. Between the 18 and 21 June, and the two sites, this shows that a plume was forecasted denser over Cape Corsica than Lampedusa two days in advance ($D+2$) and the contrary was forecasted the current day ($D+0$) or the day before ($D-1$). This may be a direct effect of a changing wind direction, strongly impacting the long range transport of dense plumes such as mineral dust plumes.

The sea salt vertical profiles show that the highest concentrations are close to the surface. This makes sense since these two sites are implemented on islands in the Mediterranean sea. The sites are thus very close to the emission sources. Compared to mineral dust, the absolute values of the concentrations are low. But, depending on the forecast lead the variability is high and from ($D-1$) to ($D+2$), the differences may be of the same order of magnitude as the concentrations. In this case, the surface variability may directly be linked to the 10 m wind speed, used in the model for the sea salt emission flux calculation.

8 Conclusions

The atmospheric composition was extensively studied in the Euro-Mediterranean region during the summer 2013, in the framework of the ADRIMED experiment (Mallet, 2015), a part of the CHARMEX project (Dulac et al., 2013). Many measurements were done and modelling studies were carried out to complement these measurements, in

ACPD
15, 10341–10388, 2015

order to have a complete analysis of the gas and aerosols behaviour. After the campaign, the WRF and CHIMERE models were used to make this analysis and results were presented in Menut et al. (2015). It was shown that the model is able to simulate the main gas and aerosols events observed during the ADRIMED period, mainly composed of mineral dust transport and sea salt over the Mediterranean. Strengths and weaknesses of the two models were quantified, including meteorology, emissions and chemistry-transport. The goal of this study is to quantify the variability of the modelled aerosols concentrations as a function of the forecast lead. The key question is *to know the reason why the model does not always forecast what was finally observed: is it due to the forecast variability increasing with time or to model biases?* The answer is certainly a bit of each, this study quantifies the relative contributions of both factors. To answer this question, the forecast variability is studied for the finally modelled aerosol concentrations, but also for all variables and processes at the origin of these concentrations: meteorology, emissions and chemistry-transport.

In order to quantify the relative impact of the models errors and the real non-linear character of the atmospheic system to represent, the first evaluation concerns the meteorology. The E-OBS database provides temperature and precipitation data (but not wind speed) in Europe. Thus scores were calculated between observations and forecasts. For the 2 m temperature, it has been shown that a bias between the model and the observations is present but that the variability from one day to the other is low, of the order of 1 % on average (Kelvin, ≈ 2 K). For precipitation, it was shown that the model reproduces the necessary information: rainfall in the right place and the right day, although the intensity remains poorly evaluated. Finally, for the wind speed, it has been shown that the variability between forecasted days is very high, of the order of several tens of %. In addition to the wind speed, the wind direction also exhibits a large variability: depending on the site and the time period, some forecast show that the wind direction may be completely different between the forecast lead, inducing transport of aerosols plumes in different directions.

ACPD
15, 10341–10388, 2015

The second evaluation was performed for surface emissions fluxes, with a focus on mineral dust and biogenic emissions, the most dependent on meteorology variability. At the first order, and according to the parameterizations used to calculate these fluxes, it clearly appear that mineral aerosols are mostly sensitive to the 10 m wind speed and biogenic emissions to 2 m temperature. The forecast variability diagnosed for these meteorological parameters is clearly reflected in the emission fluxes. Mineral dust can be highly variable from one forecasted day to another. This variability is the largest in Africa, the location of the main sources. Depending on the forecast lead and the modelled day, the variability may reach 30 %. Even for the nearest forecast ($D+0$), the variability can reach 10 %. Biogenic emissions have a lower forecast variability and the differences logically increase with the forecast: for the ($D+0$) forecast, the main difference with ($D-1$) is about 2 %, while for the ($D+2$) forecast, the main difference is about 8 %.

The last evaluation was performed for AOD and aerosols concentrations. First, an evaluation of the AOD predictability was presented and comparisons of modelled values were done with AERONET photometers measurements. Correlations showed that the model is not always able to reproduce the observed AOD for this period. This is due to the model iteself but also to the studied period length: for the same region, the same variables and with the same model, the scores are better in Menut et al. (2015), being calculated over 45 days (and 15 days in the present study). For AOD, the main conclusion is that the differences between model and observations are always higher that the differences between the several forecast leads. Comparisons were also presented as maps of differences: the differences increased with the forecast lead but the patterns show alternating negative and positive values, showing "plumes" of differences. This clearly shows the impact of the variability of the forecasted wind speed and direction. For the surface PM_{10} concentrations, the same conclusion was done: the most important differences are between observed and modelled concentrations and not between the several forecast leads. Vertical profiles were also presented for mineral dust and sea salt: for mineral dust, the largest variability is observed in altitude, mainly between

ACPD
15, 10341–10388, 2015

2000 and 4000 m, representing the long range transport. For sea salt, the largest variability is close to the surface, where the emissions occur.

Finally, there are two main conclusions for this study: (i) the differences between observations and model results remain higher than between the several forecast leads. If chemistry-transport model results are not close to the observations, this is mainly due to the forecast biases (including the meteorology) and not to its variability. (ii) Among all studied variables, the highest variability for the forecast is due to the wind speed and direction. This variable is at the origin of the mineral dust and sea salt emissions, as well as the long-range transport of these long-lived species: differences between the forecasted wind speed and directions are at the origin of the main differences between the forecasts of aerosol concentrations.

Acknowledgements. This study was partly funded by the French Ministry in charge of Ecology. We acknowledge Francois Dulac (IPSL/LSCE) and Marc Mallet for their coordination of the CHARMEX program and the ADRIMED project, respectively. We thank the EEA for maintaining and providing the AirBase database of pollutants surface concentrations over Europe. We thank the principal investigators and their staff for establishing and maintaining the AERONET sites used in this study: Didier Tanré for Banizoumbou, Capo Verde and Dakar; Bernadette Chatenet and Jean-Louis Rajot for Zinder and Cinzana; Daniela Meloni and Alcide Di Sarra for Lampedusa. We acknowledge the Service d'Observation PHOTONS/AERONET and the AERONET-ACTRIS TNA supporting the AERONET activity in Europe. We acknowledge the E-OBS dataset from the EU-FP6 project ENSEMBLES (http://ensembles-eu.metoffice.com) and the data providers in the ECAD project (http://www.ecad.eu).

References

Bessagnet, B., Hodzic, A., Vautard, R., Beekmann, M., Cheinet, S., Honoré, C., Liousse, C., and Rouil, L.: Aerosol modeling with CHIMERE: preliminary evaluation at the continental scale, Atmos. Environ., 38, 2803–2817, 2004. 10347

Borrego, C., Monteiro, A., Pay, M., Ribeiro, I., Miranda, A., Basart, S., and Baldasano, J.: How bias-correction can improve air quality forecasts over Portugal, Atmos. Environ., 45, 6629–6641, doi:10.1016/j.atmosenv.2011.09.006, 2011. 10343

ACPD

15, 10341–10388, 2015

Carslaw, K. S., Boucher, O., Spracklen, D. V., Mann, G. W., Rae, J. G. L., Woodward, S., and Kulmala, M.: A review of natural aerosol interactions and feedbacks within the Earth system, Atmos. Chem. Phys., 10, 1701–1737, doi:10.5194/acp-10-1701-2010, 2010. 10343

Chen, F. and Dudhia, J.: Coupling an advanced land surface-hydrology model with the Penn State-NCAR MM5 modeling system. Part I: Model implementation and sensitivity, Mon. Weather Rev., 129, 569–585, 2001. 10346

Curier, R., Timmermans, R., Calabretta-Jongen, S., Eskes, H., Segers, A., Swart, D., and Schaap, M.: Improving ozone forecasts over Europe by synergistic use of the LOTOS-EUROS chemical transport model and in-situ measurements, Atmos. Environ., 60, 217–226, doi:10.1016/j.atmosenv.2012.06.017, 2012. 10343

Dubovik, O. and King, M. D.: A flexible inversion algorithm for retrieval of aerosol optical properties from Sun and sky radiance measurements, J. Geophys. Res.-Atmos., 105, 20673–20696, doi:10.1029/2000JD900282, 2000. 10344

Dulac, F., Arboledas, L. A., Alastuey, A., Ancellet, G., Arndt, J., Attié, J.-L., Augustin, P., Becagli, S., Bergametti, G., Bocquet, M., Bordier, F., Bourdon, A., Bourrianne, T., Bravo-Aranda, J., Carrer, D., Ceamanos, X., Chazette, P., Chiapello, I., Comeron, A., D'Amico, G., D'Anna, B., Delbarre, H., Denjean, C., Desboeufs, K., Descloitres, J., Diouri, M., Biagio, C. D., Iorio, T. D., Sarra, G. D., Doppler, L., Durand, P., Amraoui, L. E., Ellul, R., Ferré, H., Fleury, L., Formenti, P., Freney, E., Gaimoz, C., Gerasopoulos, E., Goloub, P., Gomez-Amo, J., Granados-Munoz, M., Grand, N., Grobner, J., Rascado, J.-L. G., Guieu, C., Hadjimitsis, D., Hamonou, E., Hansson, H., Iarlori, M., Ioannou, S., Jambert, C., Jaumouillé, E., Jeannot, M., Junkermann, W., Keleshis, C., Kokkalis, P., Lambert, D., Laurent, B., Léon, J.-F., Liousse, C., Bartolome, M. L., Losno, R., Mallet, M., Mamouri, R.-E., Meloni, D., Menut, L., Montoux, N., Baquero, R. M., Nabat, P., Navas-Guzman, F., Nicolae, D., Nicolas, J., Notton, G., Ohayon, W., Paoli, C., Papayannis, A., Pelon, J., Pey, J., Pont, V., Pujadas, M., Querol, X., Ravetta, F., Renard, J.-B., Rizi, V., Roberts, G., Roujean, J.-L., Sartelet, K., Savelli, J.-L., Sciare, J., Sellegri, K., Sferlazzo, D., Sicard, M., Smyth, A., Solmon, F., Tanré, D., Torres, B., Totems, J., Sanchez, A. T., Verdier, N., Vignelles, D., Vincent, J., Wagner, F., Wang, Y., Wenger, J., and Yassaa, N.: Overview of the project ChArMEx activities on Saharan Dust in the Mediterranean region, in: 7th Int. Workshop on Sand/Duststorms and Associated Dustfall, 2–4 December 2013, Frascati, Italy, 2013. 10344, 10361

European Union: Ambient air quality and cleaner air for Europe, Directive 2008/50/EC of the European Parliament and of the Council of 21 May 2008, OJ L 152, 1–44, 2008. 10343

ACPD
15, 10341–10388, 2015

Fenger, J.: Air pollution in the last 50 years – from local to global, Atmos. Environ., 43, 13–22, 2009. 10342

Grell, G. A. and Devenyi, D.: A generalized approach to parameterizing convection combining ensemble and data assimilation techniques, Geophys. Res. Lett., 29, 1693, doi:10.1029/2002GL015311, 2002. 10347

Guenther, A., Karl, T., Harley, P., Wiedinmyer, C., Palmer, P. I., and Geron, C.: Estimates of global terrestrial isoprene emissions using MEGAN (Model of Emissions of Gases and Aerosols from Nature), Atmos. Chem. Phys., 6, 3181–3210, doi:10.5194/acp-6-3181-2006, 2006. 10348

Guerreiro, C., de Leuw, F., and Foltescu, V.: Air quality in Europe, Report, European Environment Agency, 9, 112, 2013. 10344

Hong, S. Y., Dudhia, J., and Chen, S.: A revised approach to ice microphysical processes for the bulk parameterization of clouds and precipitation, Mon. Weather Rev., 132, 103–120, 2004. 10346

Hong, S. Y., Noh, Y., and Dudhia, J.: A new vertical diffusion package with an explicit treatment of entrainment processes, Mon. Weather Rev., 134, 2318–2341, doi:10.1175/MWR3199.1, 2006. 10346

Honoré, C., Rouïl, L., Vautard, R., Beekmann, M., Bessagnet, B., Dufour, A., Elichegaray, C., Flaud, J., Malherbe, L., Meleux, F., Menut, L., Martin, D., Peuch, A., Peuch, V., and Poisson, N.: Predictability of European air quality: the assessment of three years of operational forecasts and analyses by the PREV'AIR system, J. Geophys. Res., 113, D04301, doi:10.1029/2007JD008761, 2008. 10345

Inness, A., Baier, F., Benedetti, A., Bouarar, I., Chabrillat, S., Clark, H., Clerbaux, C., Coheur, P., Engelen, R. J., Errera, Q., Flemming, J., George, M., Granier, C., Hadji-Lazaro, J., Huijnen, V., Hurtmans, D., Jones, L., Kaiser, J. W., Kapsomenakis, J., Lefever, K., Leitão, J., Razinger, M., Richter, A., Schultz, M. G., Simmons, A. J., Suttie, M., Stein, O., Thépaut, J.-N., Thouret, V., Vrekoussis, M., Zerefos, C., and the MACC team: The MACC reanalysis: an 8 yr data set of atmospheric composition, Atmos. Chem. Phys., 13, 4073–4109, doi:10.5194/acp-13-4073-2013, 2013. 10345

Mallet, M.: Overview of the Chemistry-Aerosol Mediterranean Experiment/Aerosol Direct Radiative Forcing on the Mediterranean Climate (ChArMEx/ADRIMED) summer 2013 campaign, Atmos. Chem. Phys. Discuss., in preparation, 2015. 10344, 10361

ACPD
15, 10341–10388, 2015

Mailler, S., Menut, L., di Sarra, A. G., Becagli, S., Di Iorio, T., Formenti, P., Bessagnet, B., Briant, Régis, Luis Gómez-Amo, J., Mallet, M., Rea, Géraldine, Siour, G., Sferlazzo, D. M., Traversi, R., Udisti, R., and Turquety, S.: On the radiative impact of aerosols on photolysis rates: comparison of simulations and observations in the Lampedusa island during the ChArMEx/ADRIMED campaign, Atmos. Chem. Phys. Discuss., 15, 7585–7643, doi:10.5194/acpd-15-7585-2015, 2015. 10348

Manders, A., Schaap, M., and Hoogerbrugge, R.: Testing the capability of the chemistry transport model LOTOS-EUROS to forecast {PM10} levels in the Netherlands, Atmos. Environ., 43, 4050–4059, doi:10.1016/j.atmosenv.2009.05.006, 2009. 10343

Menut, L. and Bessagnet, B.: Atmospheric composition forecasting in Europe, Ann. Geophys., 28, 61–74, doi:10.5194/angeo-28-61-2010, 2010. 10345

Menut, L., Coll, I., and Cautenet, S.: Impact of meteorological data resolution on the forecasted ozone concentrations during the ESCOMPTE IOP 2a and 2b, Atmos. Res., 74, 139–159, 2005. 10345

Menut, L., Chiapello, I., and Moulin, C.: Previsibility of mineral dust concentrations: the CHIMERE-DUST forecast during the first AMMA experiment dry season, J. Geophys. Res., 114, D07202, doi:10.1029/2008JD010523, 2009. 10345

Menut, L., Goussebaile, A., Bessagnet, B., Khvorostiyanov, D., and Ung, A.: Impact of realistic hourly emissions profiles on modelled air pollutants concentrations, Atmos. Environ., 49, 233–244, 2012. 10348

Menut, L., Bessagnet, B., Khvorostyanov, D., Beekmann, M., Blond, N., Colette, A., Coll, I., Curci, G., Foret, G., Hodzic, A., Mailler, S., Meleux, F., Monge, J.-L., Pison, I., Siour, G., Turquety, S., Valari, M., Vautard, R., and Vivanco, M. G.: CHIMERE 2013: a model for regional atmospheric composition modelling, Geosci. Model Dev., 6, 981–1028, doi:10.5194/gmd-6-981-2013, 2013a. 10347

Menut, L., Perez Garcia-Pando, C., Haustein, K., Bessagnet, B., Prigent, C., and Alfaro, S.: Relative impact of roughness and soil texture on mineral dust emission fluxes modeling, J. Geophys. Res., 118, 6505–6520, doi:10.1002/jgrd.50313, 2013b. 10348, 10354

Menut, L., Mailler, S., Siour, G., Bessagnet, B., Turquety, S., Rea, G., Briant, R., Mallet, M., Sciare, J., and Formenti, P.: Ozone and aerosols tropospheric concentrations variability analyzed using the ADRIMED measurements and the WRF-CHIMERE models, Atmos. Chem. Phys. Discuss., 15, 3063–3125, doi:10.5194/acpd-15-3063-2015, 2015. 10344, 10345, 10353, 10357, 10358, 10362, 10363

ACPD
15, 10341–10388, 2015

Millan, M., Estrela, M. J., Sanz, M. J., Mantilla, E., Martan, M., Pastor, F., Salvador, R., Vallejo, R., Alonso, L., Gangoiti, G., Ilardia, J., Navazo, M., Albizuri, A., Artano, B., Ciccioli, P., Kallos, G., Carvalho, R. A., Andreas, D., Hoff, A., Werhahn, J., Seufert, G., and Versino, B.: Climatic feedbacks and desertification: the mediterranean model, J. Climate, 18, 684–701, 2005. 10343

Mlawer, E., Taubman, S., Brown, P., Iacono, M., and Clough, S.: Radiative transfer for inhomogeneous atmospheres: RRTM a validated correlated-k model for the longwave, J. Geophys. Res., 102, 16663–16682, 1997. 10346

Monks, P., Granier, C., Fuzzi, S., Stohl, A., Williams, M., Akimoto, H., Amann, M., Baklanov, A., Baltensperger, U., Bey, I., Blake, N., Blake, R., Carslaw, K., Cooper, O., Dentener, F., Fowler, D., Fragkou, E., Frost, G., Generoso, S., Ginoux, P., Grewe, V., Guenther, A., Hansson, H., Henne, S., Hjorth, J., Hofzumahaus, A., Huntrieser, H., Isaksen, I., Jenkin, M., Kaiser, J., Kanakidou, M., Klimont, Z., Kulmala, M., Laj, P., Lawrence, M., Lee, J., Liousse, C., Maione, M., McFiggans, G., Metzger, A., Mieville, A., Moussiopoulos, N., Orlando, J., O'Dowd, C., Palmer, P., Parrish, D., Petzold, A., Platt, U., Pöschl, U., Prévôt, A., Reeves, C., Reimann, S., Rudich, Y., Sellegri, K., Steinbrecher, R., Simpson, D., ten Brink, H., Theloke, J., van der Werf, G., Vautard, R., Vestreng, V., Vlachokostas, C., and von Glasow, R.: Atmospheric composition change – global and regional air quality, Atmos. Environ., 43, 5268–5350, doi:10.1016/j.atmosenv.2009.08.021, 2009. 10342

Mulcahy, J. P., Walters, D. N., Bellouin, N., and Milton, S. F.: Impacts of increasing the aerosol complexity in the Met Office global numerical weather prediction model, Atmos. Chem. Phys., 14, 4749–4778, doi:10.5194/acp-14-4749-2014, 2014. 10343

Niu, T., Gong, S. L., Zhu, G. F., Liu, H. L., Hu, X. Q., Zhou, C. H., and Wang, Y. Q.: Data assimilation of dust aerosol observations for the CUACE/dust forecasting system, Atmos. Chem. Phys., 8, 3473–3482, doi:10.5194/acp-8-3473-2008, 2008. 10343

Pérez, I. A., Sánchez, M. L., and García, M. Á.: Weibull wind speed distribution: Numerical considerations and use with sodar data, J. Geophys. Res., 112, D20112, doi:10.1029/2006JD008278, 2007. 10343

Rouïl, L., Honoré, C., Vautard, R., Beekmann, M., Bessagnet, B., Malherbe, L., Meleux, F., Dufour, A., Elichegaray, C., Flaud, J., Menut, L., Martin, D., Peuch, A., Peuch, V., and Poisson, N.: PREV'AIR: an operational forecasting and mapping system for air quality in Europe, B. Am. Meteorol. Soc., 90, 73–83, doi:10.1175/2008BAMS2390.1, 2009. 10345

ACPD
15, 10341–10388, 2015

Spyrou, C., Kallos, G., Mitsakou, C., Athanasiadis, P., Kalogeri, C., and Iacono, M. J.: Modeling the radiative effects of desert dust on weather and regional climate, Atmos. Chem. Phys., 13, 5489–5504, doi:10.5194/acp-13-5489-2013, 2013. 10343

Turquety, S., Menut, L., Bessagnet, B., Anav, A., Viovy, N., Maignan, F., and Wooster, M.: API-FLAME v1.0: high-resolution fire emission model and application to the Euro-Mediterranean region, Geosci. Model Dev., 7, 587–612, doi:10.5194/gmd-7-587-2014, 2014. 10346, 10348

Von Storch, H., Langenberg, H., and Feser, F.: A spectral nudging technique for dynamical downscaling purposes, Mon. Weather Rev., 128, 3664–3673, 2000. 10347

Wild, O., Zhu, X., and Prather, M. J.: Fast-J: accurate simulation of in- and below-cloud photolysis in tropospheric chemical models, J. Atmos. Chem., 37, 245–282, 2000. 10348

ACPD
15, 10341–10388, 2015

Table 1. Characteristics of the AirBase and AERONET stations used in this study. Note that the AirBase Italian stations of Chitignano, Baceno, Schivenoglia and Vercelli provide daily averaged values, when all other stations provide hourly (but not regular) measurements. The altitude is in m a.s.l.

Site	Country	Longitude (°)	Latitude (°)	Altitude (m a.s.l.)
ADRIMED measurements sites				
Lampedusa	Italy	12.63	35.51	45.
Cape Corsica	France	9.41	42.83	533.
AirBase coastal "background" stations				
Zorita	Spain	−0.16	40.73	619.
Cartagena	Spain	−0.97	37.60	10.
Malaga	Spain	−4.46	36.72	36.
Ajaccio	France	8.73	41.92	28.
Bastia	France	9.44	42.69	57.
Hyeres	France	6.13	43.11	33.
Taranto	Italy	17.28	40.41	10.
Chitignano	Italy	11.90	43.66	650.
AirBase continental "background" stations				
Aranjuez	Spain	−3.59	40.04	501.
Logrono	Spain	−2.42	42.46	386.
Cordoba	Spain	−4.77	37.90	119.
Agen	France	0.62	44.19	50.
Champforgeuil	France	4.83	46.82	46.
Gap	France	6.07	44.55	741.
Baceno	Italy	8.25	46.31	1637.
Schivenoglia	Italy	11.07	44.99	16.
Vercelli	Italy	8.40	45.31	131.
AERONET stations				
Banizoumbou	Nigeria	2.66	13.54	250.
Capo Verde	Capo Verde	−22.93	16.73	60.
Dakar	Senegal	−16.95	14.39	0.
Cinzana	Mali	−5.93	13.28	285.
Ilorin	Nigeria	4.340	8.32	350.
Izana	Spain	−16.49	28.31	2391.
Forth Crete	Greece	25.27	35.31	20.
Saada	Morocco	−8.15	31.61	420.
Zinder Airport	Nigeria	8.98	13.75	456.

ACPD
15, 10341–10388, 2015

Table 2. Scores for the modelled 2 m temperature compared to the measurements. For each forecast lead, correlation R (0 : 1) and bias (in Kelvin) are presented.

Site	$(D-1)$		$(D+0)$		$(D+1)$		$(D+2)$	
	R	bias	R	bias	R	bias	R	bias
Cape Corsica	0.81	−1.21	0.81	−1.20	0.83	−1.11	0.79	−1.01
Zorita	0.80	−2.45	0.80	−2.38	0.76	−2.24	0.74	−2.01
Bastia	0.79	0.70	0.79	0.68	0.78	0.75	0.79	0.89
Chitignano	0.90	−2.58	0.90	−2.55	0.90	−2.38	0.86	−2.22
Aranjuez	0.98	−2.01	0.98	−1.95	0.97	−1.91	0.95	−1.70
LaCiguena	0.94	−2.47	0.93	−2.44	0.93	−2.36	0.90	−2.07
Cordoba	0.98	−1.95	0.98	−1.86	0.98	−1.63	0.98	−1.58
Agen	0.87	−2.11	0.86	−2.10	0.86	−1.94	0.85	−1.61
Champforgeuil	0.96	−3.73	0.96	−3.63	0.97	−3.62	0.92	−3.48
Gap	0.98	−2.21	0.98	−2.15	0.97	−1.94	0.96	−1.65
Baceno	0.96	−4.02	0.95	−3.94	0.95	−3.79	0.90	−3.60
Schivenoglia	0.94	−2.40	0.94	−2.37	0.92	−2.12	0.90	−1.90
Vercelli	0.89	−3.00	0.89	−3.01	0.85	−2.88	0.79	−2.63

ACPD
15, 10341–10388, 2015

Table 3. Scores for the modelled daily cumulated total precipitation (mm day^{-1}) compared to the measurements. For each forecast lead, Hit Rate HR and bias are presented.

Site	$(D-1)$		$(D+0)$		$(D+1)$		$(D+2)$	
	HR	bias	HR	bias	HR	bias	HR	bias
Zorita	0.67	0.26	0.67	−1.05	0.67	−5.78	0.33	−8.20
Chitignano	1.00	−0.25	1.00	−2.78	0.50	−3.17	0.50	−4.22
La Ciguena	0.80	1.48	0.80	3.09	1.00	4.06	1.00	4.95
Cordoba	1.00	1.80	1.00	1.94	0.00	−1.38	1.00	2.63
Agen	0.75	−5.73	0.75	−5.26	0.75	−2.78	0.50	−5.90
Champforgeuil	0.78	−4.17	0.89	−4.84	1.00	−4.91	0.89	−5.10
Gap	0.33	−0.60	0.33	−0.56	0.33	−1.60	1.00	1.83
Baceno	0.78	3.09	0.78	1.55	0.67	0.71	0.78	1.52
Schivenoglia	0.50	−7.80	0.50	−8.31	0.25	−8.22	0.25	−8.53
Vercelli	0.40	−1.65	0.40	−2.51	0.60	−2.71	0.60	−2.78

ACPD
15, 10341–10388, 2015

Table 4. Scores for the comparison between observed and modelled hourly AOD. For each site, n_{obs} is the number of hourly valid AERONET AOD observations. $\overline{AOD}$ is the mean AOD value averaged over the whole period for observations and model. The statistical scores presented are the correlation R, the root mean square error RMSE and the bias.

Site (n_{obs})	$\overline{AOD}$		R	RMSE	Bias
	obs	mod			
Banizoumbou (151)					
($D-1$)	0.486	0.353	0.115	0.408	−0.133
($D+0$)	0.486	0.351	0.108	0.409	−0.135
($D+1$)	0.486	0.364	0.125	0.407	−0.122
($D+2$)	0.486	0.379	0.154	0.401	−0.107
Capo Verde (75)					
($D-1$)	0.421	0.338	0.343	0.170	−0.083
($D+0$)	0.421	0.337	0.335	0.171	−0.084
($D+1$)	0.421	0.353	0.134	0.182	−0.069
($D+2$)	0.421	0.350	0.448	0.154	−0.071
Dakar (145)					
($D-1$)	0.587	0.806	0.612	0.321	0.218
($D+0$)	0.587	0.793	0.615	0.315	0.206
($D+1$)	0.587	0.764	0.539	0.291	0.177
($D+2$)	0.587	0.760	0.384	0.334	0.173
Izana (234)					
($D-1$)	0.035	0.092	0.929	0.073	0.056
($D+0$)	0.035	0.090	0.912	0.072	0.055
($D+1$)	0.035	0.084	0.975	0.054	0.049
($D+2$)	0.035	0.091	0.806	0.085	0.056
Lampedusa (88)					
($D-1$)	0.138	0.166	0.889	0.092	0.028
($D+0$)	0.138	0.166	0.889	0.093	0.028
($D+1$)	0.138	0.165	0.852	0.092	0.026
($D+2$)	0.138	0.154	0.805	0.089	0.015
Saada (176)					
($D-1$)	0.242	0.147	0.421	0.173	−0.094
($D+0$)	0.242	0.146	0.424	0.173	−0.095
($D+1$)	0.242	0.136	0.343	0.183	−0.106
($D+2$)	0.242	0.137	0.244	0.202	−0.105
Zinder (155)					
($D-1$)	0.450	0.713	0.221	0.537	0.264
($D+0$)	0.450	0.714	0.230	0.534	0.264
($D+1$)	0.450	0.785	0.460	0.538	0.335
($D+2$)	0.450	0.863	0.603	0.566	0.413
Forth Crete (32)					
($D-1$)	0.099	0.118	0.619	0.054	0.019
($D+0$)	0.099	0.115	0.627	0.054	0.016
($D+1$)	0.099	0.119	0.584	0.060	0.020
($D+2$)	0.099	0.120	0.486	0.065	0.021

ACPD
15, 10341–10388, 2015

Table 5. Scores for the comparison between observed and modelled hourly PM_{10} surface concentrations ($\mu g\,m^{-3}$). For each site, n_{obs} is the number of hourly valid PM_{10} observed surface concentrations. $\overline{PM_{10}}$ is the mean PM_{10} value averaged over the whole period for observations and model. The statistical scores presented are the correlation R, the root mean square error RMSE and the bias.

Site (n_{obs})	$\overline{PM_{10}}$		R	RMSE	Bias
	obs	mod			
Lampedusa (428)					
($D-1$)	37.902	23.825	0.399	24.487	−14.077
($D+0$)	37.902	23.690	0.401	24.558	−14.212
($D+1$)	37.902	23.234	0.419	24.659	−14.668
($D+2$)	37.902	23.118	0.382	25.104	−14.784
Zorita (359)					
($D-1$)	15.827	10.397	0.490	11.016	−5.431
($D+0$)	15.827	10.292	0.482	10.927	−5.536
($D+1$)	15.827	8.322	0.022	11.489	−7.506
($D+2$)	15.827	10.312	0.500	11.604	−5.515
Ajaccio (432)					
($D-1$)	21.676	21.717	0.075	10.915	0.041
($D+0$)	21.676	21.809	0.101	10.891	0.133
($D+1$)	21.676	21.570	0.100	10.989	−0.106
($D+2$)	21.676	21.961	0.143	11.355	0.286
Bastia (428)					
($D-1$)	21.600	18.083	0.043	15.730	−3.518
($D+0$)	21.600	18.177	0.045	15.798	−3.424
($D+1$)	21.600	18.306	0.085	15.607	−3.295
($D+2$)	21.600	18.442	0.058	15.794	−3.158
Hyeres (426)					
($D-1$)	26.115	16.439	0.456	13.880	−9.676
($D+0$)	26.115	16.391	0.440	13.982	−9.724
($D+1$)	26.115	16.521	0.387	14.112	−9.594
($D+2$)	26.115	17.512	0.473	13.127	−8.603

ACPD
15, 10341–10388, 2015

Table 5. Continued.

Site (n_{obs})	$\overline{PM_{10}}$		R	RMSE	Bias
	obs	mod			
Cordoba (426)					
($D-1$)	20.261	10.139	0.148	12.432	−10.121
($D+0$)	20.261	10.136	0.142	12.448	−10.125
($D+1$)	20.261	10.416	0.232	12.392	−9.845
($D+2$)	20.261	12.202	0.276	13.393	−8.059
Agen (432)					
($D-1$)	13.866	14.597	0.101	12.253	0.731
($D+0$)	13.866	14.239	0.069	11.543	0.373
($D+1$)	13.866	13.331	0.020	10.803	−0.534
($D+2$)	13.866	12.871	0.167	9.556	−0.995
Champforgeuil (421)					
($D-1$)	12.216	13.755	0.435	8.309	1.539
($D+0$)	12.216	13.715	0.419	8.466	1.498
($D+1$)	12.216	13.966	0.455	8.489	1.750
($D+2$)	12.216	14.856	0.471	9.263	2.640
Gap (427)					
($D-1$)	13.691	8.618	0.553	7.320	−5.073
($D+0$)	13.691	8.414	0.552	7.453	−5.277
($D+1$)	13.691	8.397	0.498	7.654	−5.294
($D+2$)	13.691	9.259	0.487	7.288	−4.432

ACPD
15, 10341–10388, 2015

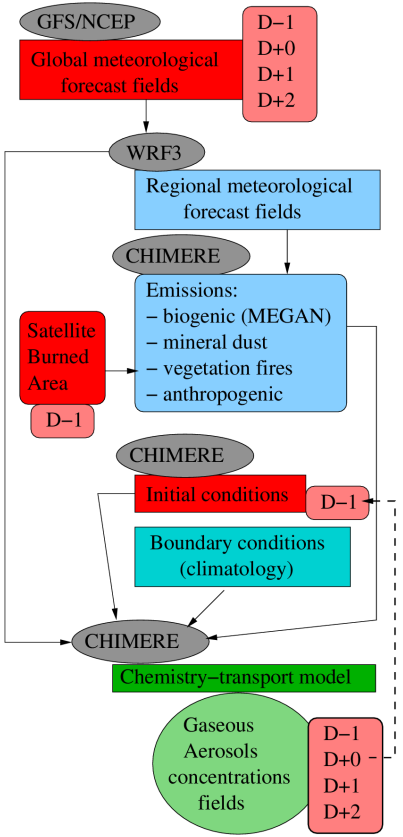

Figure 1. The forecast modelling system. This system includes the download of global meteorological fields, the simulations of the regional models WRF and CHIMERE, and the calculation of numerous emissions fluxes for gas and aerosols species and corresponding to anthropogenic, biogenic, vegetation fires, sea salt and mineral dust emissions. Each day, four days are modelled and the current day ($D + 0$) is used as initialization for the next day forecast ($D - 1$).

ACPD
15, 10341–10388, 2015

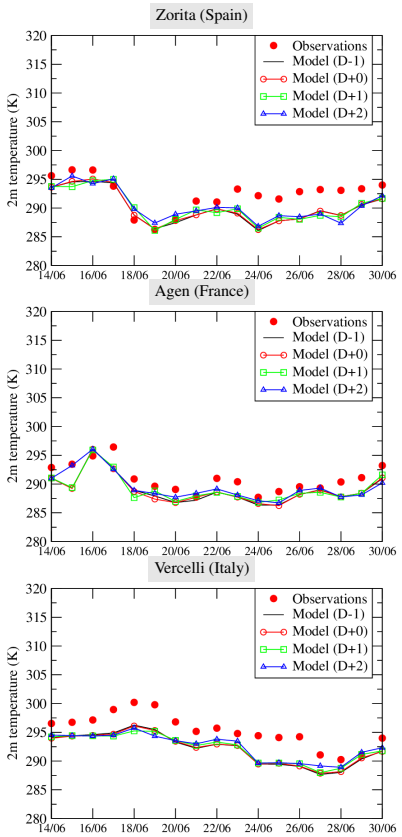

Figure 2. Time series of 2 m temperature (K) observed with E-OBS and modelled with WRF and for the forecast leads ($D - 1$) to ($D + 2$).

ACPD
15, 10341–10388, 2015

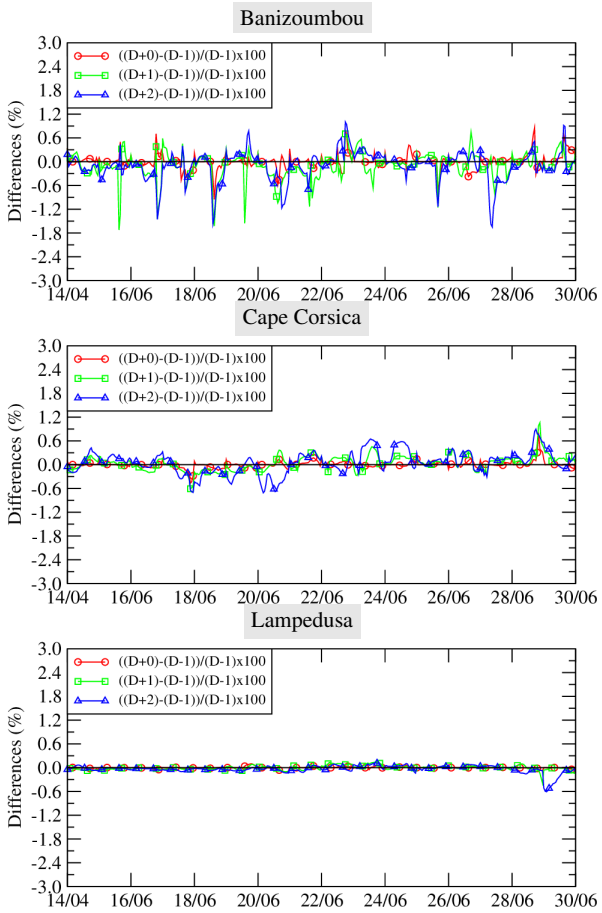

Figure 3. Time series of hourly modelled 2 m temperature differences for several sites. Each line corresponds to a difference between the forecast ($D+0$), ($D+1$) or ($D+2$) and the simulation of the day before ($D-1$). Results are expressed in percentages of differences.

ACPD
15, 10341–10388, 2015

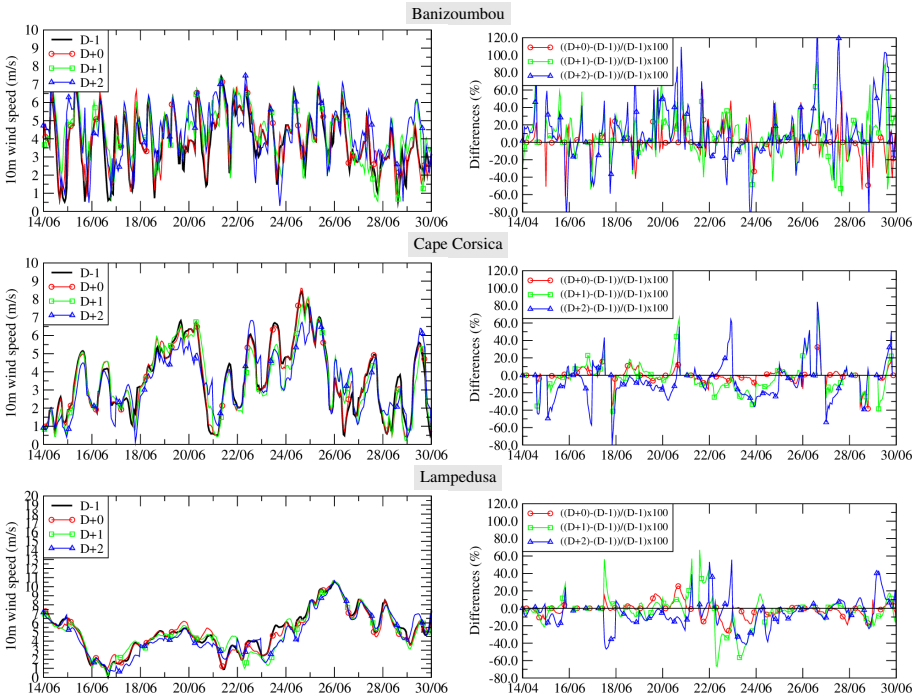

Figure 4. (left) Time series of hourly 10 m wind speed ($m\,s^{-1}$) for the sites of Banizoumbou, Cape Corsica and Lampedusa and for several forecast leads. (right) Relative differences (%) between these wind speed values. Values are presented only when $|U|_{(D-1)} > 2\,m\,s^{-1}$ to avoid too large and unrealistic values in case of low wind speed.

ACPD
15, 10341–10388, 2015

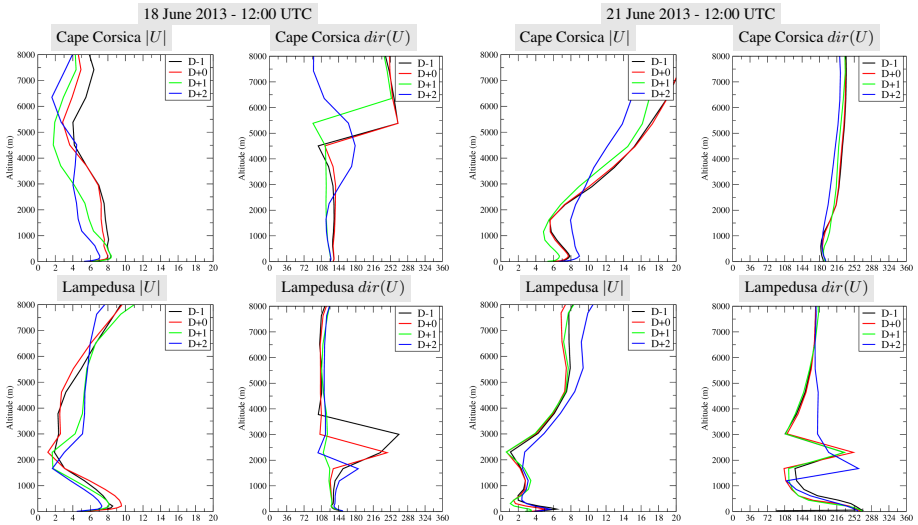

Figure 5. Modelled vertical profiles of the wind speed ($m\,s^{-1}$) for the cells corresponding to the locations of Cape Corsica and Lampedusa. Profiles are presented for the 18 and 21 June 2013 at 12:00 UTC and for the four forecast leads, from ($D-1$) to ($D+2$).

ACPD
15, 10341–10388, 2015

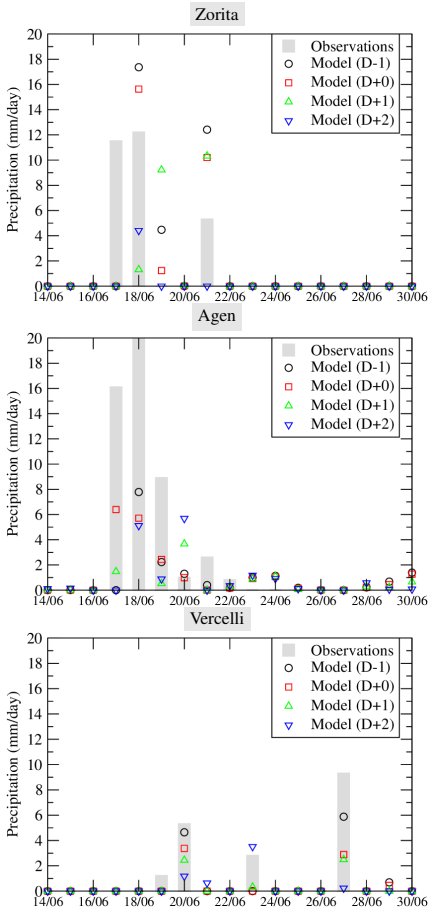

Figure 6. Time series of total precipitation (mm day^{-1}) observed with E-OBS and modelled with WRF and for the forecast leads (D – 1) to (D + 2).

ACPD
15, 10341–10388, 2015

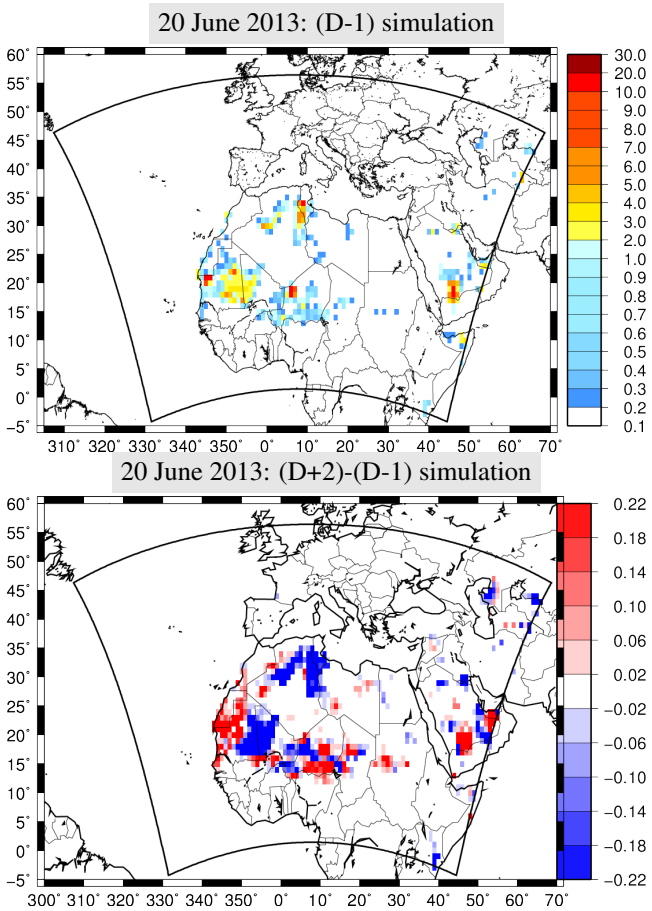

Figure 7. (top) Map of mineral dust fluxes for the 20 June 2013 and the forecast ($D-1$) ($g\,m^{-2}\,day^{-1}$), (bottom) absolute differences ($D+2$)–($D-1$) for the 20 June 2013.

ACPD
15, 10341–10388, 2015

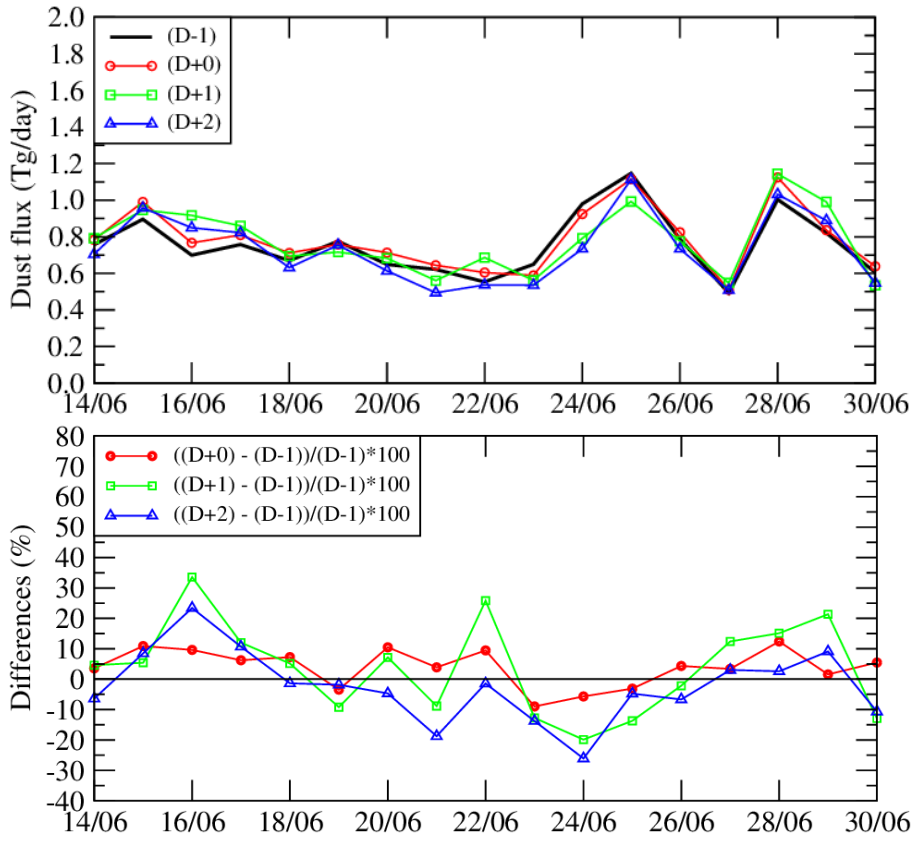

Figure 8. (top) Time series of daily mineral dust fluxes, spatially cumulated over the modelled domain. Units are in Tg day^{-1}. (bottom) Differences between the flux expressed percentages.

ACPD
15, 10341–10388, 2015

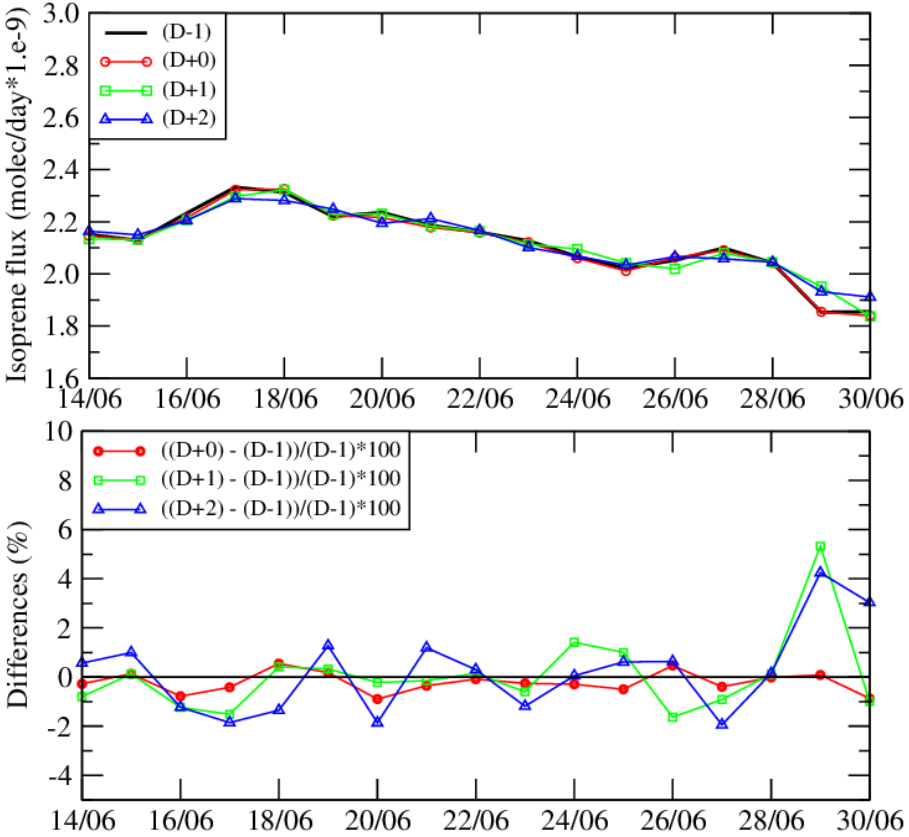

Figure 9. (top) Time series of the daily isoprene fluxes, spatially cumulated over the modelled domain. Units are in 10^9 molecules day^{-1}. (bottom) Differences between the flux expressed percentages.

ACPD
15, 10341–10388, 2015

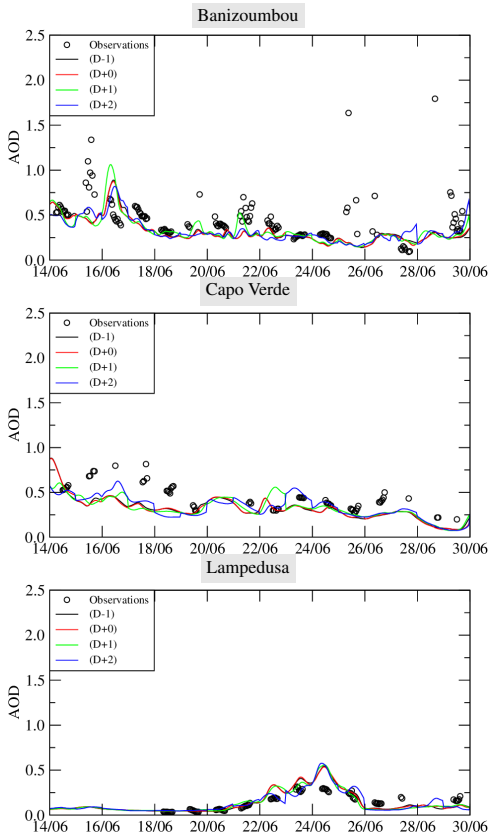

Figure 10. Time series of Aerosol Optical Depth (AOD) for the sites of Banizoumbou, Capo Verde and Lampedusa. Values are displayed for the AERONET observations (symbols) and the modelled values for the several forecast leads: ($D-1$), ($D+0$), ($D+1$) and ($D+2$).

ACPD
15, 10341–10388, 2015

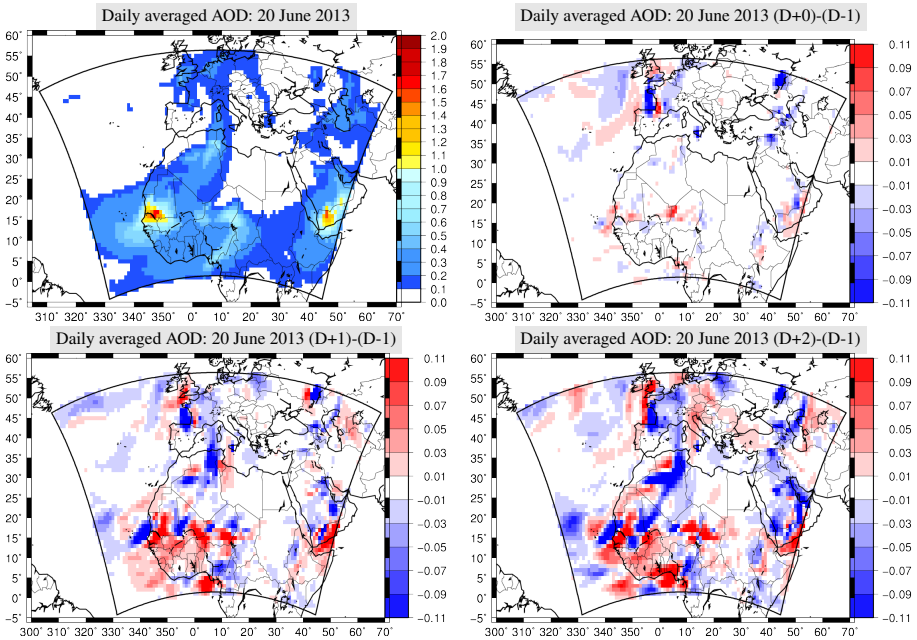

Figure 11. Map of modelled (D – 1) AOD for the 20 June 2013 and maps of AOD differences between the several forecast leads.

ACPD
15, 10341–10388, 2015

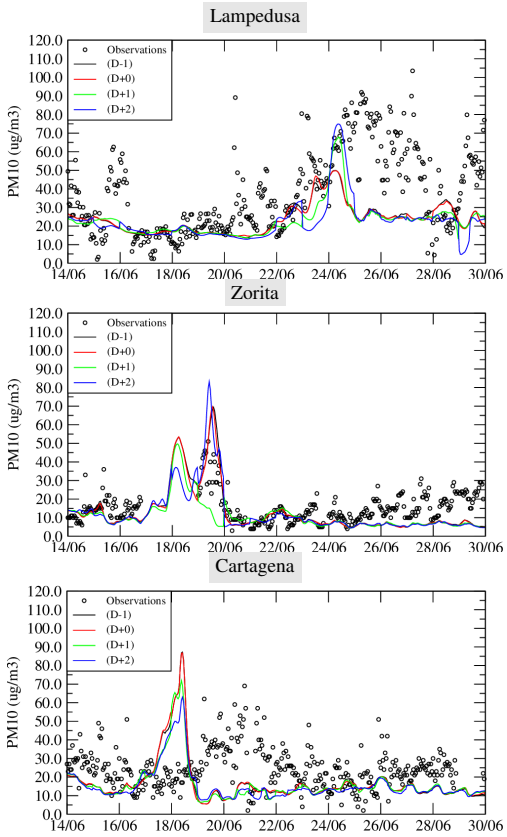

Figure 12. Time series of hourly surface concentrations of PM_{10} (in $\mu g m^{-3}$) for the sites of Lampedusa, Zorita and Cartagena. Observations are from the EEA network as symbols and the four model forecast leads are as colored lines.

ACPD
15, 10341–10388, 2015

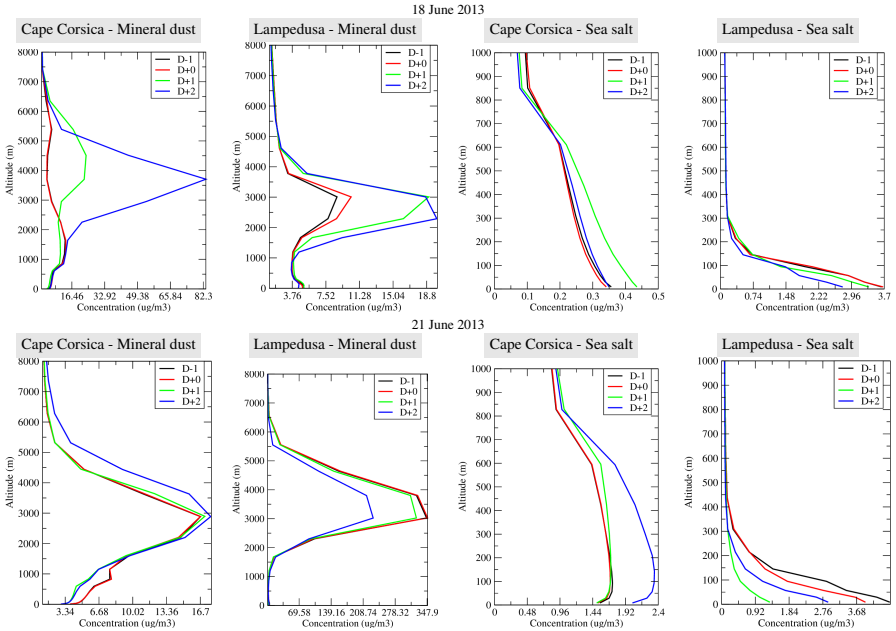

Figure 13. Vertical profiles of mineral dust and sea salt concentrations ($\mu g\,m^{-3}$). In each figure, the four forecast leads are presented from ($D-1$) to ($D+2$). Results are presented for Cape Corsica and Lampedusa and for the 18 and 21 June 2013.

ACPD
15, 10341–10388, 2015